Supplementary Information

High-Performance Organic Solar Cells Enabled by P-i-N Structure and Ternary Strategy

Ju Zhao, [a] Jiabin Zhang, [a] Yuejia Dou, [a] Kai Zhang, *[a] Chang Zhu, [a] Zuiyi Zhong [a] and Fei Huang *[a]

[a] Institute of Polymer Optoelectronic Materials and Devices, Guangdong Basic Research Center of Excellence for Energy & Information Polymer Materials, State Key Laboratory of Luminescent Materials and Devices, South China University of Technology, Guangzhou 510640, P. R. China

E-mail address: mszhangk@scut.edu.cn (K. Zhang); msfhuang@scut.edu.cn (F. Huang).

* Corresponding Authors

Experimental Methods

1.Materials and experimental procedures

Materials

PBQx-TF, ZY-4Cl was purchased from Solarmer Materials Inc. DT-Y6 and PNDIT-F3N was purchased from Dongguan Volt Ampere Photoelectric Technology Co., Ltd. PEDOT:PSS ((CLEVIOS P VP AI 4083) was purchased from Heraeus. The alcohol-soluble conjugated polymer PNDIT-F3N was synthesized in our lab according to the reported literature[1]. All solvents and materials were commercially available and used received.

Device fabrication

The devices were fabricated with conventional structures of ITO/PEDOT:PSS/active layer/PNDIT-F3N/Ag. The ITO substrates were cleaned sequentially by detergent, deionized water, and isopropanol under sonication, and then dried at 65 ℃ in a baking oven. After being treated with oxygen plasma, PEDOT: PSS layer (~30 nm) was spin-coated on the top of ITO and annealed in the air at 150 °C for 15 min. For the BHJ film, the active materials were dissolved in toluene (Tol) at 80 °C for 2 hours. The system of PBQx-TF:DT-Y6, PBQx-TF: DT-Y6:ZY-4Cl with a ratio of 1:1.2 and 1:0.9:0.3, respectively (PBQx-TF=6mg/mL). The blend solvent was spin-coated at 2000 rpm for PBQx-TF:DT-Y6 and 2500 rpm for PBQx-TF:DT-Y6:ZY-4Cl. Then all the films were annealed at 100 °C for 10 min. For the LBL film, the PBQx-TF was dissolved in *o*-XY with a concentration of 8 mg/ mL at 80 °C for 2 hours.

For the binary system, the acceptor DT-Y6 with a concentration of 7.2 mg/ mL was dissolved in Tol at 60 °C for 2 hours. For the ternary system, the DT-Y6:ZY-4Cl (0.75:0.25) with a total concentration of 7.2 mg/ mL was dissolved in Tol at 60 °C for 2 hours. Then the donor was spin-coated on the PEDOT:PSS to form a 60 nm film, and the acceptor was spin-coated to form a 50 nm film. Afterward, a ~10 nm PNDIT-F3N was spin-coated on the active layer as an electron transport layer. Finally, 100 nm Ag was deposited by thermal vacuum evaporation under 10^{-6} mbar and finally obtained a 0.0516 cm^2 active area device. The effective area of the device was confined to 0.04 cm^2 by a non-refractive mask to improve the accuracy of measurements.

2.Measurements and characterization

Photovoltaic performance measurement: The current density-voltage (*J-V*) curves of devices were recorded by a Keithley 2400 source meter under 1 sun, AM 1.5 G spectra from a solar simulator (Taiwan, Enlitech). The light intensity was 100 $mW \cdot cm^{-2}$ as calibrated by a China General Certification Center (CGC) certified reference monocrystal silicon cell (Enlitech).

External quantum efficiency (EQE): The EQE spectra were measured by the Enlitech QE-R3011 measurement system.

UV-Vis spectra: UV-Vis absorption spectra were recorded by a PerkinElmer Lambda UV-Vis spectrophotometer.

SCLC measurements: For single-carrier devices, those devices were fabricated to measure hole and electron mobility by using the SCLC method. The hole-only device structures were ITO/PEDOT:PSS/active layer/MoO3/Ag. The electron-only device structures were ITO/ZnO/Active layer/PNDIT-F3N/Ag. The charge carrier mobility was determined by fitting the dark current to the model of a single-carrier SCLC according to the equations[2]: $J=(9/8)\varepsilon_0\varepsilon_r\mu V^2 d^{-3}$ and $V=V_{appl}-V_{bi}-V_s$, where J is the current density, d is the film thickness of the active layer, μ is the charge carrier mobility, ε_r is the relative dielectric constant of the transport medium, ε_0 is the permittivity of free space, V_{appl} is the applied voltage and V_{bi} is the offset voltage. The carrier mobility can be calculated from the slope of the $J^{1/2}$–V curves.

Photo-CELIV, C−V, EIS, and Capacitance-frequency (C-ω) measurements: Photo-CELIV, C-ω, and EIS were obtained from a platform namely PAIOS which contains the characterization of Solar Cells and OLED. Photo-CELIV measurements (ramp rate 200 V ms^{-1}, delay time: 0 s, offset voltage: 0 V, lightpulse length: 100 μs) were also performed using PAIOS for different light intensities. C−V measurements were tested within the voltage range

from -3 V to 2 V under dark condition. The Mott-Shottky equation is described as the equation of $\frac{1}{C^2} = \frac{2(V_{bi} - V)}{A^2 q \varepsilon_r \varepsilon_0 N}$, C is the capacitance value, V is the applied voltage, A is the device area, q is the elementary charge, ε_r is the relative permittivity, ε_0 is the vacuum permittivity, and N is the charge carrier density[3]. EIS measurements were conducted using a commercially available PAIOS. The measurements were performed using conditions that had an applied bias of open-circuit voltage of OPV in the dark, and a frequency ranging from 10 MHz to 1 Hz. The *C-ω* measurement was performed from 10 MHz to 1 Hz under dark environment. Mott-Schottky measurement was tested within the voltage range from -3 V to 2 V under dark conditions.

TPV, TPC measurements: The transient photocurrent and transient photovoltage characteristics of devices were measured by applying 500 nm laser pulses with a pulse width of 120 fs and low pulse energy to the short-circuit devices in the dark. The laser pulses were generated from an optical parametric amplifier (TOPAS-Prime) pumped by a mode-locked Ti: sapphire oscillator seeded regenerative amplifier with a pulse energy of 1.3 mJ at 800 nm and a repetition rate of 1 kHz (Spectra Physics Spitfire Ace). The charge extraction time was extracted from the fitting line of the TPC signal with the equation: $\delta I = Aexp(t/T)$, where A is a constant that fits the peak high, t is time, and T is the charge extraction time. The transient photovoltage was tested under the open-circuit condition to explore the photovoltage decay. The photovoltage decay kinetics of all devices follow a mono-exponential decay: $\delta V = Aexp(-t/T)$, where t is the time, and T is the charge carrier lifetime.

Vertical component distribution characterization: The surface energy of films was obtained by VCA15 surface contact angle analyzer (Data physics). The depth-profile data were obtained with a time of flight secondary ion mass spectrometry (TOF-SIMS) (ION-TOF GmbH, Germany) instrument in negative mode (sputter condition: a 2.5 keV Bi^{3+} beam; Area: 300 μm ×300 μm; analysis condition: a 30 keV Bi^{3+} beam; Area: 150 μm×150 μm)[4].

Atomic force microscope (AFM) measurement: AFM measurements were performed by a Digital Instrumental DI Multimode Nanoscope III in a taping mode.

Transmission electron microscopy (TEM) measurement: TEM measurements were conducted by JEM-2100F instrument.

Grazing incidence Wide Angle X-ray Scattering (GIWAXS) measurement: GIWAXS measurements were performed by Xeuss 2.0 SAXS/WAXS laboratory beamline using a Cu X-ray source (8.05 keV, 1.54 Å) and a Pilatus3R 300K detector.

***E*$_{loss}$ measurement:** the highly sensitive EQE was conducted by an integrated system with a Fourier transform photocurrent meter (QE Pro and NIR Quest 512, Ocean Optics)[5]. Electroluminescence quantum efficiency (EQE_{EL}) was tested by applying an external current/voltage source through the OSCs (REPS-Pro, Enlitech).

3.Supplementary Figures and Tables

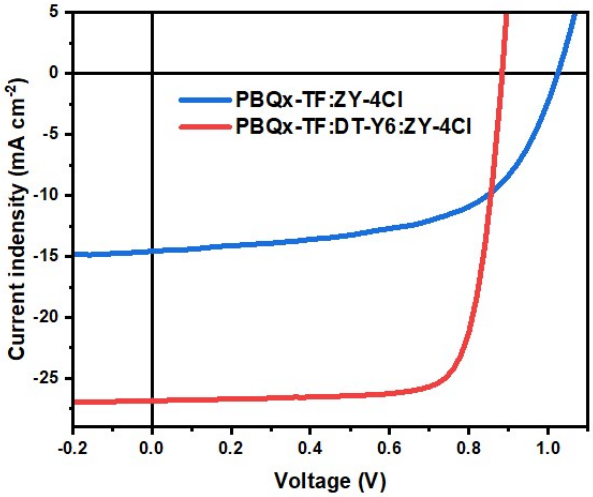

Fig. S1 The J-V curves of PBQx-TF: ZY-4Cl and PBQx-TF: DT-Y6: ZY-4Cl

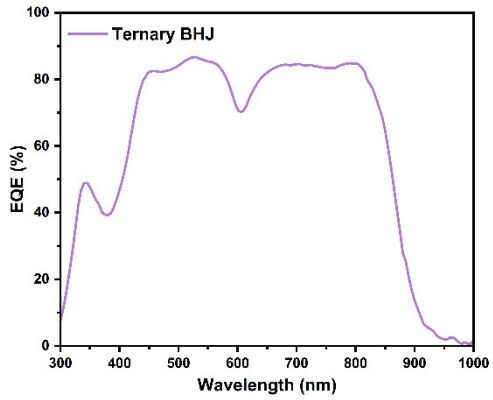

Fig. S2 The EQE spectra of PBQx-TF: DT-Y6: ZY-4Cl.

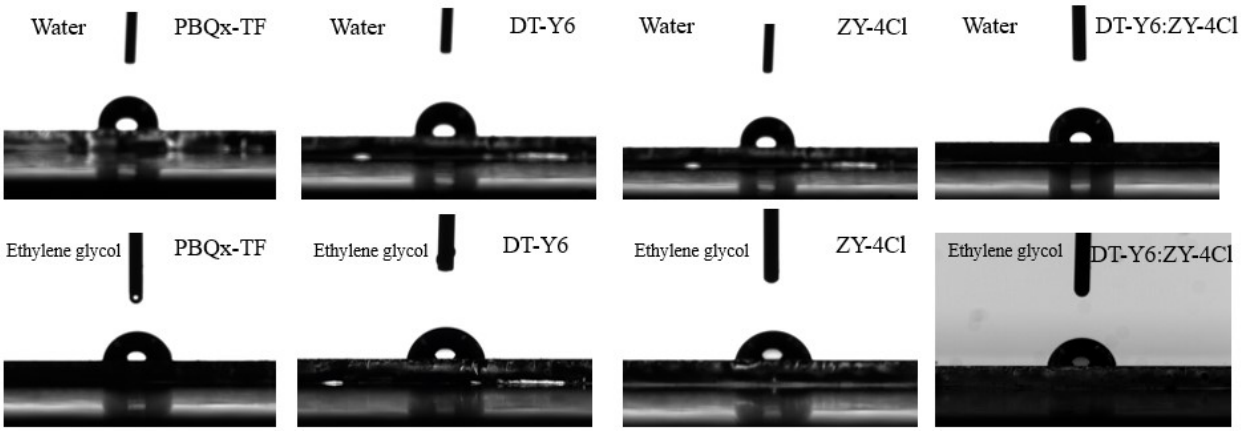

Fig. S3 Contact angle images of pristine PBQx-TF, DT-Y6, ZY-4Cl and DT-Y6: ZY-4Cl with water and ethylene glycol droplets on top

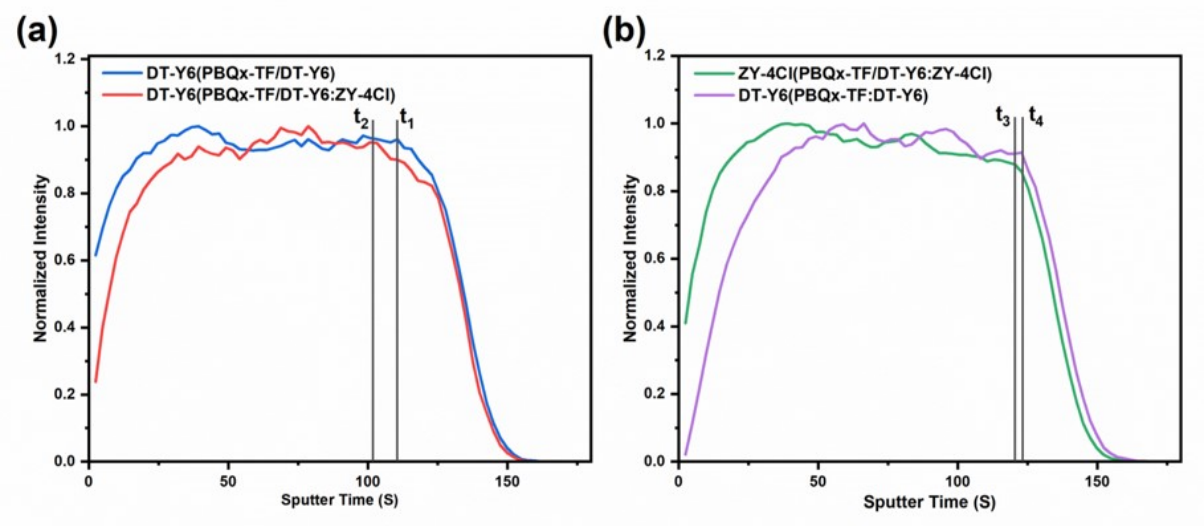

Fig. S4 (a) The acromion sputtering time of DT-Y6 in binary LBL and ternary LBL devices. (b) The acromion sputtering time of DT-Y6 in binary BHJ device and ZY-4Cl in ternary LBL device.

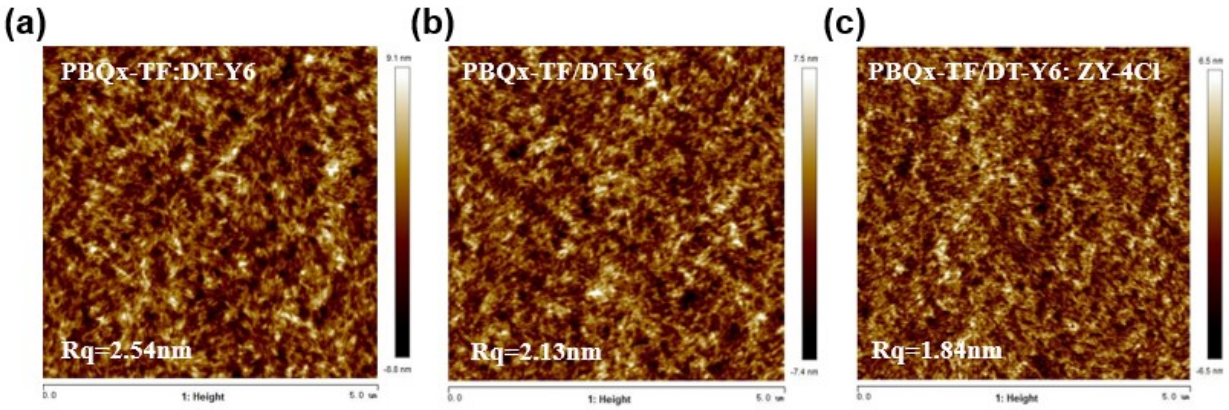

Fig. S5 (a-c) AFM height images of corresponding films.

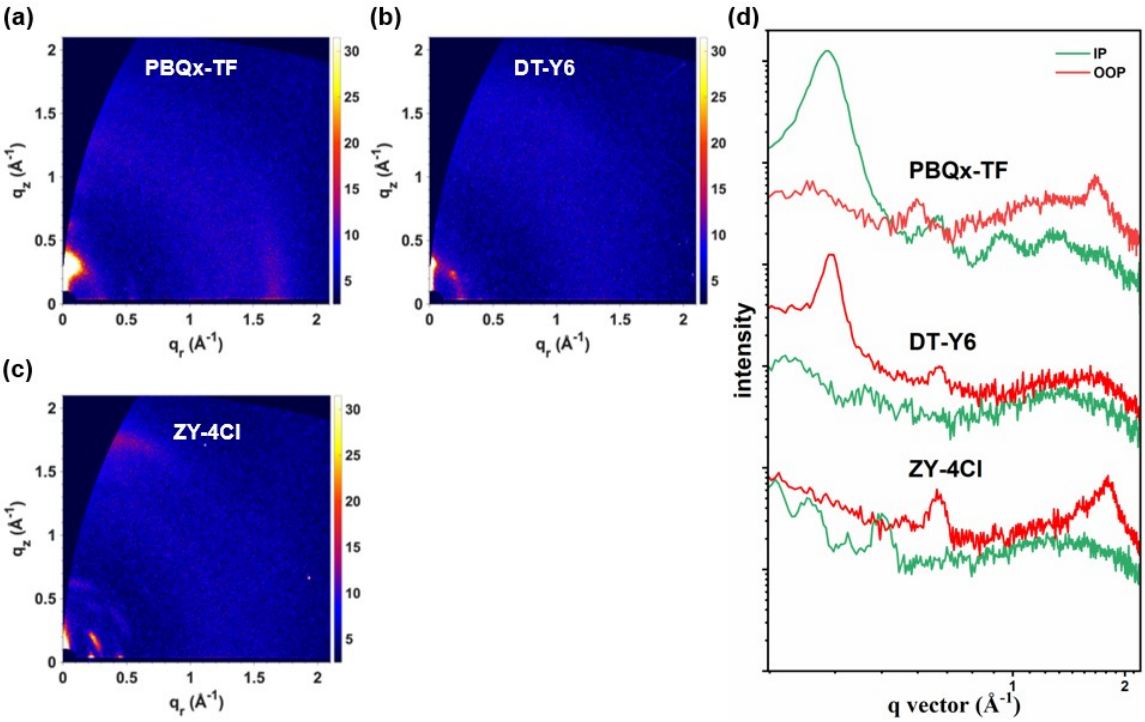

Fig. S6 (a-c) 2D GIWAXS patterns of corresponding films. (d) 1D profiles of corresponding films.

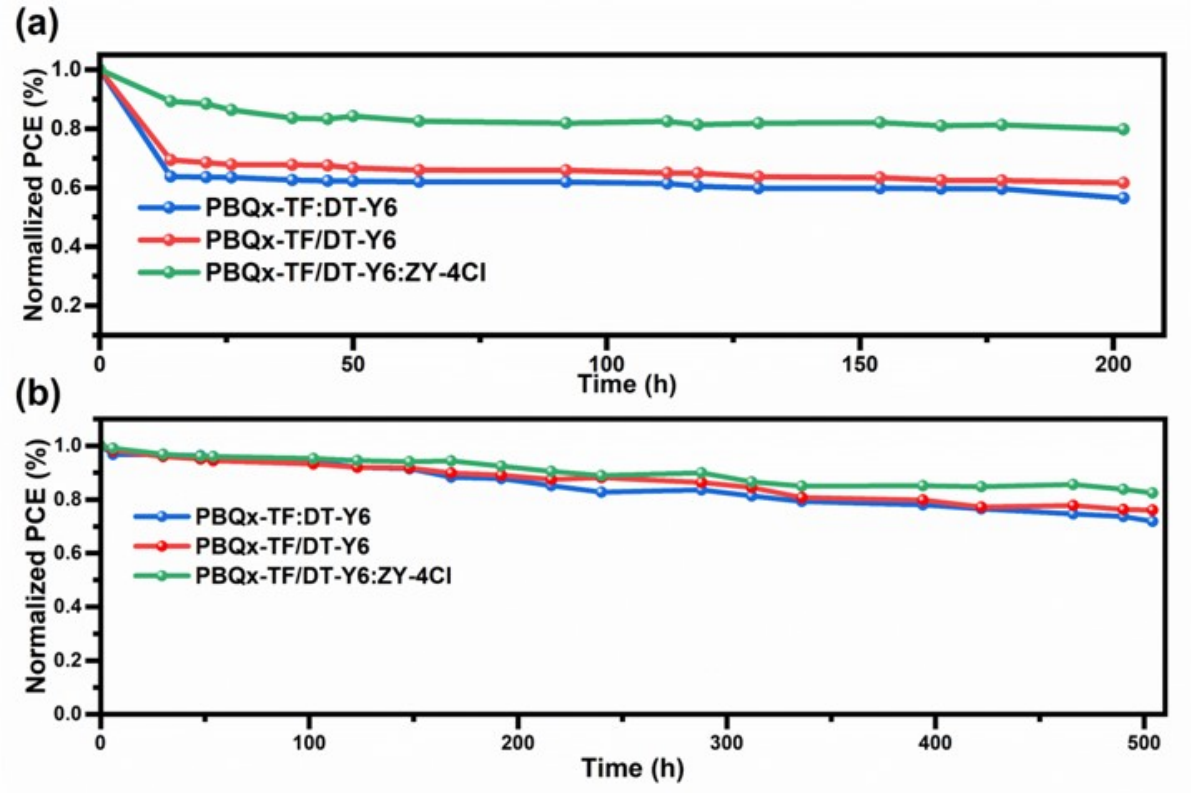

Fig. S7 (a) Photostability of each device under the simulated illumination of 100 mW cm^{-2}. (b) Thermal stability of each device under 65 ºC in the glove box.

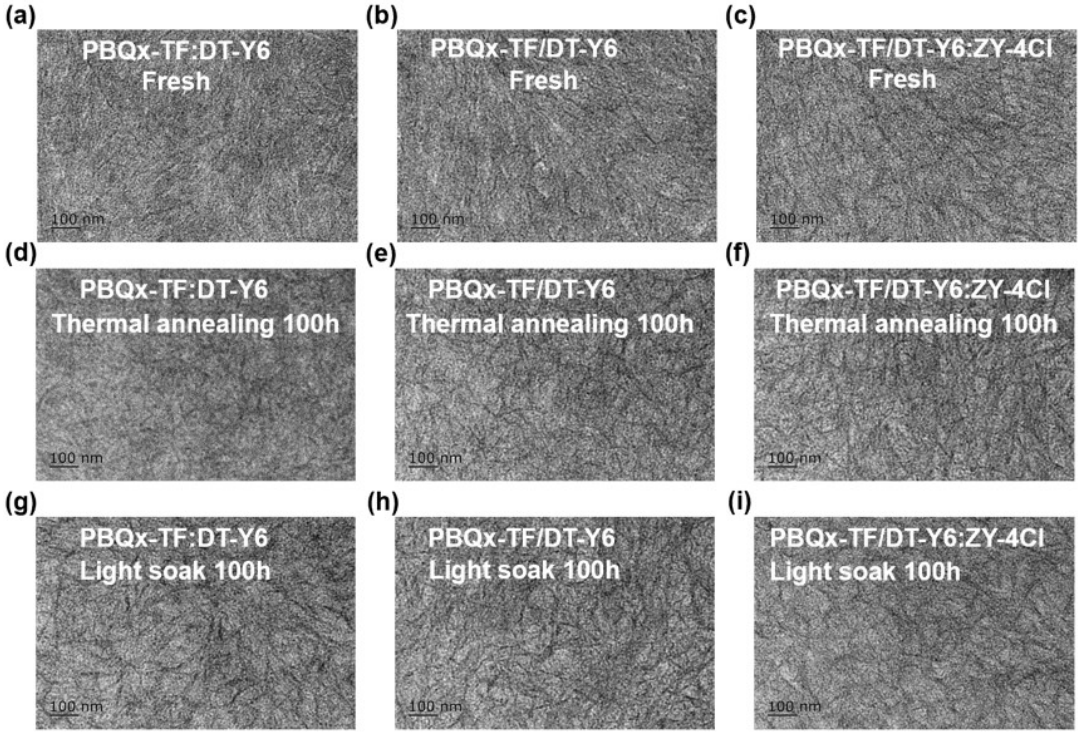

Fig. S8 TEM images for blend films after heating or illumination.

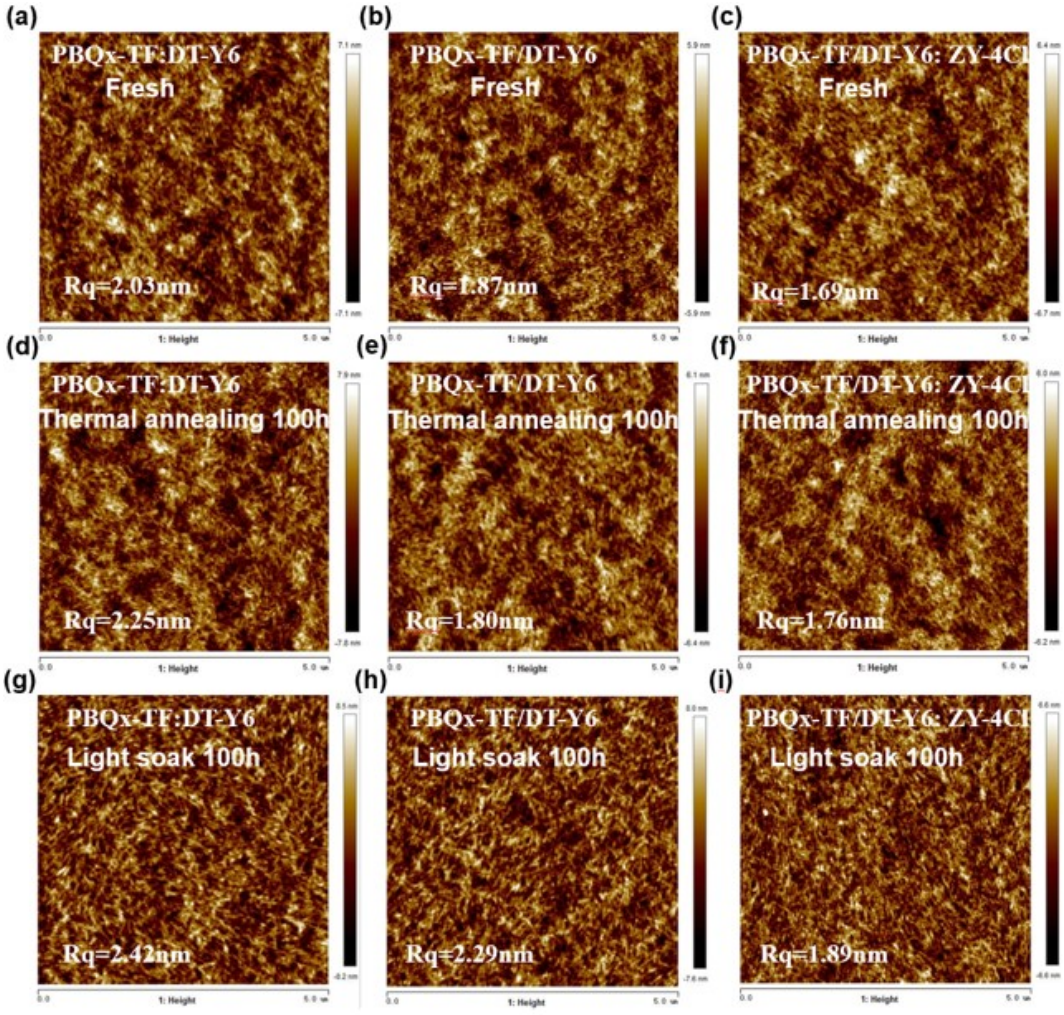

Fig. S9 AFM images for blend films after heating or illumination.

Table S1 The representative recent works on ternary BHJ and LBL OSCs

	Active layer	V_{OC} (V)	J_{SC} (mA cm-2)	FF (%)	PCE (%)	ref
BHJ	PM6:L8-BO:PY-IT	0.882	25.81	78.9	17.97	[6]
	PM6:ec9:PY-IT	0.858	26.78	79.2	18.19	[7]
	D18:T9TBO-F:Y6-O	0.87	26.93	78.07	18.29	[8]
	PM6:L8-BO:BTP-eC9	0.886	27.22	79.5	19.17	[9]
	PM6:BTTC:BTP-eC9	0.853	28.32	79.40	19.18	[10]
	PM6:CH8-6:L8-BO	0.884	27.46	78.6	19.2	[11]
	PM6:eC9:PCT-4Cl	0.865	27.90	79.8	19.25	[12]
	PM6:ITOA:BTP-eC9	0.866	28.33	78.79	19.33	[13]
	PB2:HLG:BTP-eC9	0.883	27.3	80.8	19.5	[14]
	PM6:D18:L8-BO	0.896	26.7	81.9	19.6	[15]
	PM6:PBTz-F:L8-BO	0.907	27.10	80.06	19.68	[16]
	D18:LJ1:L8-BO	0.924	26.84	79.12	19.78	[17]
	D18:Z8:L8-BO	0.92	27.2	80.8	20.2	[18]
LBL	PM6/L8-BO:PY-IT	0.876	26.66	80.1	18.70	[6]
	D18/BS3TSe-4F:Y6-O	0.845	29.41	76.56	19.03	[19]
	D18/T9TBO-F:Y6-O	0.87	27.9	78.81	19.13	[8]
	PM1:D18/L8-BO	0.90	27.2	78.53	19.13	[20]
	D18/L8-BO:ec9	0.88	27.63	78.9	19.18	[21]
	PM6/ec9:PY-IT	0.859	27.79	81.3	19.41	[7]
	PDTP-BDD:D18/L8-BO	0.905	26.90	79.53	19.36	[22]
	PBQx-TF/DT-Y6:ZY-4Cl	0.881	27.45	80.43	19.46	This work
	D18/L8-BO	0.908	26.39	81.59	19.55	[23]

T**able S2** Photovoltaic parameters of each device under simulated illumination of AM 1.5G, 100 mW cm^{-2}.

Active layer	V_{OC} (V)	J_{SC} (mA cm^{-2})	FF(%)	PCE (%)
PBQx-TF:ZY-4Cl	1.021 (1.009±0.011)	14.57 (12.80±1.55)	58.56 (58.68±0.11)	8.76 (7.59±0.99)

Table S3 The hole and electron mobilities of each device.

Device	μ_h (cm^2 V^{-1} s^{-1})	μ_e (cm^2 V^{-1} s^{-1})	μ_h/μ_e
PBQx-TF:DT-Y6	5.10×10^{-4}	3.61×10^{-4}	1.41
PBQx-TF/DT-Y6	6.13×10^{-4}	5.01×10^{-4}	1.22
PBQx-TF/ DT-Y6:ZY-4Cl	6.64×10^{-4}	5.81×10^{-4}	1.14

Table S4 Fitting parameters of for impedance spectra of each device

Device	$R_{transport}$ (Ω)	$C_{transport}$ (nF)	$R_{recombination}$ (Ω)	$C_{recombination}$ (nF)	R_S (Ω)
PBQx-TF: DT-Y6	1520	1.85	901	3.06	15.49
PBQx-TF/ DT-Y6	1210	1.93	727	3.06	12.26
PBQx-TF/ DT-Y6: ZY-4Cl	793	1.12	419	1.32	7.86

Table S5 Trap DOS of each device

Device	N_t (cm^{-3})	E_ω (eV)
PBQx-TF:DT-Y6	1.15×10^{17}	0.51
PBQx-TF/DT-Y6	8.26×10^{16}	0.51
PBQx-TF/DT-Y6:ZY-4Cl	8.27×10^{16}	0.50

Table S6 Contact angles of water and ethylene glycol on films and surface energy values calculated by Owens method.

Surface	θ_{Water} [°]	θ_{EG} [°]	γ^d [mN m^{-1}]	γ^p [mN m^{-1}] [a]	γ [mN m^{-1}] [b]
PBQx-TF	102.3	83.2	10.16	8.64	18. 8
DT-Y6	98.4	77.2	12.06	9.18	21.24
ZY-4Cl	95.2	77.8	9.36	12.44	21.8
DT-Y6:ZY-4Cl	96.6	77.5	10.46	10.98	21.44

[a] γ^d and γ^p represent the surface free energies generated from the dispersion forces and the polar forces, respectively; [b] $\boldsymbol{\gamma=\gamma^d+\gamma^p}$

Table S7 Interfacial energy ($\gamma_{x:y}$) of each sample

	PBQx-TF:DT-Y6	PBQx-TF:ZY-4Cl	DT-Y6:ZY-4Cl
$\gamma_{x:y}$	0.178k	0.717k	0.831k

The wetting coefficient (δ) of ZY-4Cl is calculated by:

$$\delta_{ZY-4Cl} = \frac{\gamma_{PBQx-TF:ZY-4Cl} - \gamma_{DT-Y6:ZY-4Cl}}{\gamma_{PBQx-TF:DT-Y6}}$$

Table S8 Molecular packing parameters of corresponding films.

Sample	Peak	Peak location (Å^{-1})	π-π stacking distance (Å)	FWHM (Å^{-1})	Crystal coherence length (Å)
PBQx-TF	(100) In IP	0.31	\	0.044	128.45
	(010) In OOP	1.67	3.76	0.11	51.38
DT-Y6	(100) In IP	0.25	\	0.051	110.82
	(010) In OOP	1.59	3.94	1.72	3.28
ZY-4Cl	(100) In IP	0.282	\	0.024	235.5
	(010) In OOP	1.77	3.54	0.21	26.91
PBQx-TF:DT-Y6	(100) In IP	0.294	\	0.061	92.65
	(010) In OOP	1. 70	3.69	0.22	25.69
PBQx-TF/DT-Y6	(100) In IP	0.301	\	0.050	113.04
	(010) In OOP	1.71	3.67	0.18	31.40
PBQx-TF/DT-Y6:ZY-4Cl	(100) In IP	0.300	\	0.052	108.69
	(010) In OOP	1.72	3.65	0.17	33.24

1. Z. Wu, C. Sun, S. Dong, X.-F. Jiang, S. Wu, H. Wu, H.-L. Yip, F. Huang and Y. Cao, *J. Am. Chem. Soc.*, 2016, **138**, 2004-2013.

2. C. Katagiri and K. Nakayama, *Appl. Phys. Express*, 2018, **11**, 011601.
3. I. Zonno, A. Martinez-Otero, J.-C. Hebig and T. Kirchartz, *Phys. Rev. Appl.*, 2017, **7**, 034018.
4. J. Jing, S. Dong, K. Zhang, B. Xie, J. Zhang, Y. Song and F. Huang, *Nano Energy*, 2022, **93**, 106814.
5. J. Zhang, Q. Zhou, J. Xie, J. Zhao, J. Yu, K. Zhang, T. Jia, F. Huang and Y. Cao, *Adv. Funct. Mater.*, 2024, **34**, 2313722.
6. R. Gui, K. Xian, Y. Shi, W. Zhang, J. Qiao, Z. Fu, J. Wang, F. Cui, Q. Wang, V. K. Wong, P. Lu, S. K. So, M. Zhang, L. Ye, G. Li, X. Hao and H. Yin, *Adv. Energy Mater.*, 2023, **13**, 2302029.
7. Y. Zhang, W. Deng, C. E. Petoukhoff, X. Xia, Y. Lang, H. Xia, H. Tang, H. T. Chandran, S. Mahadevan, K. Liu, P. W. K. Fong, Y. Luo, J. Wu, S.-W. Tsang, F. Laquai, H. Wu, X. Lu, Y. Yang and G. Li, *Joule*, 2024, **8**, 509-526.
8. K. Jiang, J. Zhang, C. Zhong, F. R. Lin, F. Qi, Q. Li, Z. Peng, W. Kaminsky, S.-H. Jang, J. Yu, X. Deng, H. Hu, D. Shen, F. Gao, H. Ade, M. Xiao, C. Zhang and A. K. Y. Jen, *Nat. Energy*, 2022, **7**, 1076-1086.
9. W. Su, X. Zhou, Z.-F. Yao, H. Bai, Y. Duan, R. Sun, Y. Wu, Q. Wu, H. Qin, C. Zhao, W. Zhu, H. Y. Woo, J. Min, Y. Li, W. Ma and Q. Fan, *Adv. Funct. Mater.*, 2024, **34**, 2313744.
10. J. Li, C. Zhang, X. Sun, H. Wang, H. Hu, K. Wang and M. Xiao, *Nano Energy*, 2024, **125**, 109542.
11. Z. Zhang, S. Yuan, T. Chen, J. Wang, Y.-Q.-Q. Yi, B. Zhao, M. Li, Z. Yao, C. Li, X. Wan, G. Long, B. Kan and Y. Chen, *Energy. Environ. Sci.*, 2024, **17**, 5719-5729.
12. D. Luo, L. Zhang, J. Zeng, T. Dai, L. Li, W.-Y. Wong, B. Xu, E. Zhou, Y. Chen and A. K. K. Kyaw, *Nano Energy*, 2024, **125**, 109583.
13. C. Zhang, X. Zhong, X. Sun, J. Lv, Y. Ji, J. Fu, C. Zhao, Y. Yao, G. Zhang, W. Deng, K. Wang, G. Li and H. Hu, *Adv. Sci.*, 2024, **11**, 2401313.
14. Y. Wang, S. Zhang, J. Wang, J. Ren, J. Qiao, Z. Chen, Y. Yu, X.-T. Hao and J. Hou, *ACS Energy Letters*, 2024, **9**, 2420-2427.
15. L. Zhu, M. Zhang, J. Xu, C. Li, J. Yan, G. Zhou, W. Zhong, T. Hao, J. Song, X. Xue, Z. Zhou, R. Zeng, H. Zhu, C.-C. Chen, R. C. I. MacKenzie, Y. Zou, J. Nelson, Y. Zhang, Y. Sun and F. Liu, *Nat. Mater.*, 2022, **21**, 656-663.
16. T. Zhou, W. Jin, Y. Li, X. Xu, Y. Duan, R. Li, L. Yu and Q. Peng, *Adv. Sci.*, 2024, **11**, 2401405.
17. X. Jiang, X. Wang, Y. Wang, G. Ran, W. Liu, H. Lu, H. Li, N. Wei, Z. Wei, Y. Lin, Z. Ma, Y. Liu, W. Zhang, X. Xu and Z. Bo, *Adv. Funct. Mater.*, 2024, 2406744.
18. Y. Jiang, S. Sun, R. Xu, F. Liu, X. Miao, G. Ran, K. Liu, Y. Yi, W. Zhang and X. Zhu, *Nat. Energy*, 2024, **9**, 975-986.
19. W. Gao, F. Qi, Z. Peng, F. R. Lin, K. Jiang, C. Zhong, W. Kaminsky, Z. Guan, C.-S. Lee, T. J. Marks, H. Ade and A. K. Y. Jen, *Adv. Mater.*, 2022, **34**, 2202089.
20. Z. Liu, M. Zhang, L. Zhang, S. Y. Jeong, S. Geng, H. Y. Woo, J. Zhang, F. Zhang and X. Ma, *Chem. Eng. J.*, 2023, **471**, 144711.
21. Y. Xie, C. Zhou, X. Ma, S. Y. Jeong, H. Y. Woo, F. Huang, Y. Yang, H. Yu, J. Li, F. Zhang, K. Wang and X. Zhu, *Adv. Energy Mater.*, 2024, **14**, 2400013.
22. Y. He, W. Jing, C. Liao, X. Xu, Y. Duan, R. Li, L. Yu and Q. Peng, *Chem. Eng. J.*, 2024, **490**, 151920.
23. M. Xie, L. Zhu, J. Zhang, T. Wang, Y. Li, W. Zhang, Z. Fu, G. Zhao, X. Hao, Y. Lin, H. Zhou, Z. Wei and K. Lu, *Adv. Energy Mater.*, 2024, **14**, 2400214.